Heat Mass Transfer (2014) 50:1275–1290
DOI 10.1007/s00231-014-1333-1

ORIGINAL

Interaction of surface radiation with conjugate mixed convection from a vertical channel with multiple discrete heat sources

Shrikant D. Londhe · C. Gururaja Rao

Received: 9 November 2012 / Accepted: 18 March 2014 / Published online: 30 March 2014

Abstract Important results of a numerical study performed on combined conduction–mixed convection–surface radiation from a vertical channel equipped with three identical flush-mounted discrete heat sources in its left wall are provided here. The channel has walls of identical height with the spacing varied by varying its aspect ratio (AR). The cooling medium is air that is considered to be radiatively transparent. The heat generated in the channel gets conducted along its walls before getting dissipated by mixed convection and radiation. The governing equations for fluid flow and heat transfer are considered without boundary layer approximations and are transformed into vorticity–stream function form and are later normalized. The resulting equations are solved, along with relevant boundary conditions, making use of the finite volume method. The computer code written for the purpose is validated both for fluid flow and heat transfer results with those available in the literature. Detailed parametric studies have been performed and the effects of modified Richardson number, surface emissivity, thermal conductivity and AR on various pertinent results have been looked into. The significance of radiation in various regimes of mixed convection has been elucidated. The relative contributions of mixed convection and radiation in carrying the mandated cooling load have been thoroughly explored.

S. D. Londhe · C. Gururaja Rao (✉)
Department of Mechanical Engineering, National Institute of Technology, Warangal 506004, AP, India
e-mail: cgr_gcr@yahoo.co.in

List of symbols

AR	Aspect ratio (L/W)
A_{r1}, A_{r2}	Geometric ratios, W/t and W/L_h, respectively
$\bar{C}_f$	Mean friction coefficient
F_{ik}	View factor from the *i*th element to *k*th element of an enclosure
Gr_w^*	Modified Grashof number $[(g\ \beta\ \Delta T_{ref}\ W^3)/\nu_f^2]$
g	Acceleration due to gravity (9.81 m/s^2)
J_i	Radiosity of a given element i of the enclosure (W/m^2)
J_i'	Non-dimensional radiosity of a given element i of the enclosure $[J_i/(\sigma\ T_\infty^4)]$
k_f	Thermal conductivity of air (W/m K)
k_s	Thermal conductivity of channel wall as well as heat source (W/m K)
L, L_h	Heights of channel wall and heat source, respectively (m)
M_1	Grid number at the top end of the first heat source in the wall
M_2	Grid number at the bottom end of the second heat source in the wall
M_3	Grid number at the top end of the second heat source in the wall
M_4	Grid number at the bottom end of the third heat source in the wall
M_5	Total number of grids along the wall
M, N	Total number of grids in X and Y directions, respectively
n	Total number of elements of the enclosure
N_{RF}	Radiation-flow interaction parameter $[\sigma\ T_\infty^4/(k_f\ \Delta T_{ref}/W)]$
Pe_w	Peclet number based on the width of the channel (Re_wPr) or ($u_\infty W/\alpha$)
Pr_f	Prandtl number of air (ν_f/α)

$q_{cond,x,in}$ Conduction heat transfer into an element along the wall (W)
$q_{cond,x,out}$ Conduction heat transfer out of an element along the wall (W)
q_{conv} Convection heat transfer from an element of the wall (W)
q_{gen} Heat generated in an element of the wall (W)
q_{rad} Radiation heat transfer from an element of the wall (W)
q_v Rate of volumetric heat generation in each discrete heat source (W/m^3)
Re_w Reynolds number based on the width of the channel ($u_\infty W/\nu_f$)
Ri_w^* Modified Richardson number based on the width of the channel ($g\beta\Delta T_{ref} W/u_\infty^2$) or ($Gr_w^*/Re_w^2$)
t Thickness of channel walls (m)
T Local temperature in the computational domain (K or °C)
T_{max} Maximum temperature in the computational domain (K or °C)
T_∞ Free stream temperature of air (K or °C)
u, v Vertical and horizontal components of velocity, respectively (m/s)
u_∞ Free stream velocity of air (m/s)
U Non-dimensional vertical velocity of air (u/u_∞) or ($\partial\psi/\partial Y$)
V Non-dimensional horizontal velocity of air (v/u_∞) or ($-\partial\psi/\partial X$)
W Width or spacing of the channel (m)
x, y Vertical and horizontal distances, respectively (m)
X, Y Non-dimensional vertical and horizontal distances, x/W and y/W, respectively

Greek symbols

α Thermal diffusivity of air (m^2/s)
β Isobaric cubic expansivity of air $[-(1/\rho)(\partial\rho/\partial T)_p]$ (K^{-1})
γ Thermal conductance parameter $[k_f W/(k_s t)]$
ε Surface emissivity of the walls of the channel
θ Non-dimensional local temperature $[(T - T_\infty)/\Delta T_{ref}]$
θ_{av} Non-dimensional average temperature
θ_{max} Non-dimensional maximum temperature
ν_f Kinematic viscosity of air (m^2/s)
σ Stefan–Boltzmann constant (5.6697×10^{-8} W/m^2 K^4)
ψ Non-dimensional stream function $[\psi'/(u_\infty W)]$
ψ' Stream function (m^2/s)
ω Non-dimensional vorticity ($\omega' W/u_\infty$)
ω' Vorticity (s^{-1})

Miscellaneous symbols

Δx_{hs} Height of the element in the heat source portion of the wall
ΔX_{hs} Non-dimensional height of the element in the heat source portion of the wall
ΔT_{ref} Modified reference temperature difference ($q_v L_h t/k_s$) (K or °C)

1 Introduction

The classical geometry of a vertical parallel-plate channel has been explored by many researchers and the literature provides results of numerous analytical, numerical and experimental studies concerning this geometry. The first ever reported work of this kind is credited to Elenbaas [1], who, in his benchmark paper, reported the experimental results of free convection in a vertical symmetrically heated isothermal channel with air as the cooling agent. Among those researchers, who addressed mixed convection in channels, Tao [2] appears to be the first, who analytically solved the problem of mixed convection pertaining to fully-developed laminar flow in a vertical channel with a constant axial wall temperature gradient. Quintiere and Mueller [3] presented approximate analytical solutions for constant-property laminar mixed convection between finite vertical parallel plates. Bar-Cohen and Rohsenow [4] reported some useful composite relations for the average Nusselt number for natural convection in a vertical channel for both symmetric and asymmetric isothermal or isoflux boundary conditions. Aung and Worku [5] studied, numerically, laminar mixed convection in parallel-plate vertical channel for the case of asymmetric but uniform wall heat fluxes. Hamadah and Wirtz [6] solved, analytically, the problem of laminar fully-developed mixed convection in a vertical parallel-plate channel with opposing buoyancy. The problem of combined free and forced convection flow in a vertical parallel-plate channel in the fully developed region has been analyzed by Barletta [7] taking into account the effect of viscous dissipation.

With regard to multi-mode heat transfer problems involving channel geometry, prominent among the initial studies has been that of Carpenter et al. [8], who numerically probed into the interaction of surface radiation with developing laminar free convection flow between two vertical flat plates that are provided with asymmetric but uniform heat fluxes. Anand et al. [9] numerically studied the effect of wall conduction on free convection between asymmetrically heated vertical plates for the case of uniform wall temperature. Kim and Anand [10] numerically studied laminar developing fluid flow and heat transfer between a series of conducting parallel plates with surface-

mounted heat generating blocks making use of air as the cooling agent. Watson et al. [11] performed a numerical study of laminar mixed convection between a series of vertically aligned parallel plates provided with planar heat sources.

Gururaja Rao et al. [12] solved, numerically, the problem of conjugate mixed convection with surface radiation from a vertical channel with a solitary discrete heat source in each wall. They solved the problem considering a wide range of governing independent parameters, which included aspect ratio (AR), modified Richardson number, surface emissivity and thermal conductivity. Subsequently, the geometry of vertical channel with symmetric and asymmetric uniform heat generation in the two walls has also been tackled by Gururaja Rao et al. [13]. Olsson [14] predicted Nusselt number and flow rate for the case of buoyancy driven flow in a vertical parallel-plate channel, where he even looked into the influence of Rayleigh number and plate separation on the fluid flow rate. Antonio Campo et al. [15] probed, numerically, into laminar natural convection of low Prandtl number fluids (liquid metals) between vertical parallel-plate channels with isoflux heating condition. They even compared their numerical results with available experimental results from the literature. Gururaja Rao [16] solved, numerically, combined conduction–convection–radiation in a vertical channel with multiple discrete heat sources in the left wall, with detailed demonstration of the interactive effects of surface radiation on various pertinent results. Guimaraes and Menon [17] studied mixed convection in an oblique rectangular channel with three discrete heat sources provided in the bottom wall of the channel. Ermolaev and Zhbanov [18] analyzed mixed convection in a vertical plane-parallel channel with two heat sources of finite dimensions located on one of the walls making use of a two-dimensional numerical simulation. Ramjee and Satyamurty [19] studied forced convection heat transfer between parallel plates kept at unequal wall temperatures assuming laminar, incompressible, steady flow of a Newtonian fluid of constant thermophysical properties. Terekhov and Ekaid [20] made numerical investigation of laminar free convection heat transfer in a vertical parallel-plate channel with asymmetric heating.

Sakurai et al. [21] probed into the effects of radiation on turbulent mixed convection in a horizontal channel through direct numerical simulation. Al-Amri and El-Shaarawi [22] reported the effect of surface radiation on developing laminar mixed convection flow of a transparent gas through an asymmetrically heated vertical parallel-plate channel. Alves and Altemani [23] investigated, numerically, conjugate forced convection cooling of a parallel-plate channel using steady state air flow with constant properties in the laminar regime. Amirouche and Bessaïh [24] summarized results of simulation studies on three-dimensional conjugate turbulent natural convection occurring in a vertical channel that contains five cubic heat sources. Madhusudhana [25] carried out three-dimensional numerical study on natural convection in a vertical channel with flush-mounted discrete heaters on opposite conductive substrate walls and presented flow and heat transfer characteristics for various Grashof numbers. Li et al. [26] documented numerical solutions regarding the effect of surface radiation on laminar air flow taking place in a vertical and asymmetrically heated channel.

A detailed review of the literature pertaining to multimode heat transfer involving a vertical channel, as briefly summarized above, reveals that the geometry of a vertical channel comprising multiple discrete heat sources and involved in conjugate mixed convection with surface radiation has not been adequately explored. In view of the above, the present paper takes up a numerical investigation into the problem of conduction–mixed convection–radiation in a vertical channel equipped with multiple and identical flush-mounted discrete heat sources in its left wall. Here, the problem would be solved considering the pertinent fluid flow and heat transfer equations in their full strength (without the accompanying boundary layer approximations) without the simplistic assumption of fully developed flow generally made in this class of problems. A computer code would be specifically written to solve the problem and the paper aims to provide a detailed account of certain salient findings out of the studies thus carried out.

2 Problem definition and mathematical formulation

Figure 1 shows the schematic of the geometry considered in the present study together with the system of coordinates. It comprises a vertical parallel-plate channel of height L and width (or spacing) W, with each plate (or wall) of thickness t ($\ll$L). An AR is defined as L/W. Thus, for a given height L of the channel, a smaller AR implies a widely spaced channel, while a larger AR indicates narrower (or closely spaced) channel. The walls are of thermal conductivity k_s and surface emissivity ε. The left wall of the channel is equipped with three identical flush-mounted discrete heat sources, each of height L_h, while the right wall does not possess any heat sources in it. The heat sources are located at the bottom, center and top of the left wall with q_v indicating the volumetric heat generation in the three heat sources. The cooling agent used is air, which is assumed to be radiatively transparent, and it enters the channel from the bottom, as shown, at a characteristic velocity u_∞ and characteristic temperature T_∞. The top, left and bottom surfaces of the left wall and the top, right

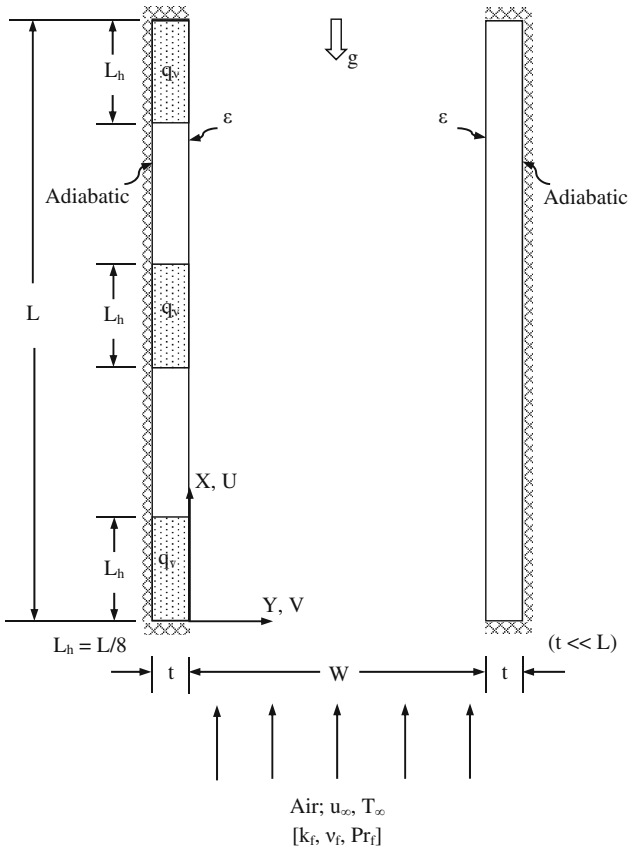

Fig. 1 Vertical parallel-plate channel with multiple heat sources in the left wall considered for study

and bottom surfaces of the right wall are considered adiabatic. Thus, the heat generated in the three heat sources of the left wall gets conducted through the wall and subsequently gets dissipated by mixed (combined free and forced) convection and radiation. The right wall of the channel merely acts as a heat sink and receives heat from the heat generating left wall, while air receives the heat by both mixed convection and radiation. Air is assumed to be of constant thermo physical properties with the Boussinesq approximation considered to be valid.

The governing equations for fluid flow and heat transfer are the continuity equation, the x and y momentum equations and the energy equation. These equations are initially converted from primitive variables form into vorticity–stream function (ω–ψ) form. The resulting equations turn out to be:

Vorticity transport equation:

$$u\frac{\partial\omega'}{\partial x}+v\frac{\partial\omega'}{\partial y}=-g\beta\frac{\partial T}{\partial y}+\nu\left(\frac{\partial^2\omega'}{\partial x^2}+\frac{\partial^2\omega'}{\partial y^2}\right) \tag{1}$$

Stream function equation:

$$\frac{\partial^2\psi'}{\partial x^2}+\frac{\partial^2\psi'}{\partial y^2}=-\omega' \tag{2}$$

Energy equation:

$$u\frac{\partial T}{\partial x}+v\frac{\partial T}{\partial y}=\alpha\left(\frac{\partial^2 T}{\partial x^2}+\frac{\partial^2 T}{\partial y^2}\right) \tag{3}$$

These equations are non-dimensionalised using normalizing parameters, viz., $X = x/W$, $Y = y/W$, $U = u/u_\infty$, $V = v/u_\infty$, $\psi = \psi'/(u_\infty W)$, $\omega = (\omega' W)/u_\infty$ and $\theta = (T - T_\infty)/\Delta T_{ref}$, where ΔT_{ref} is a modified reference temperature difference defined as $(q_v L_h t)/k_s$. This results in the following set of non-dimensionalised governing equations:

$$U\frac{\partial\omega}{\partial X}+V\frac{\partial\omega}{\partial Y}=-Ri_w^*\frac{\partial\theta}{\partial Y}+\frac{1}{Re_w}\left(\frac{\partial^2\omega}{\partial X^2}+\frac{\partial^2\omega}{\partial Y^2}\right) \tag{4}$$

$$\frac{\partial^2\psi}{\partial X^2}+\frac{\partial^2\psi}{\partial Y^2}=-\omega \tag{5}$$

$$U\frac{\partial\theta}{\partial X}+V\frac{\partial\theta}{\partial Y}=\frac{1}{Pe_w}\left(\frac{\partial^2\theta}{\partial X^2}+\frac{\partial^2\theta}{\partial Y^2}\right) \tag{6}$$

Here, Ri_w^* is the modified Richardson number, which is the principal governing parameter that helps in identifying the flow regime. A larger value of Ri_w^* signifies asymptotic free convection limit and a smaller value of the same implies asymptotic forced convection limit, while $Ri_w^* \approx 1$ stands for pure mixed convection. The Eqs. (4–6), obtained as above, are solved subject to the appropriate boundary conditions on ψ, ω and θ. An extended computational domain, as shown in Fig. 2, is used in order to capture the fluid flow and heat transfer more effectively. As can be seen, the height of the computational domain is twice the height (L) of the channel, while the width of the computational domain is equal to that of the channel (W) itself. The same figure also shows the various boundary conditions used. The temperature boundary conditions along the left and right walls of the channel are obtained through energy balance on heat generated, conducted, convected and radiated. As an example, the energy balance on a typical element pertaining to the heat source portions (other than their ends) of the left wall gives:

$$q_{gen}+q_{cond,x,in}=q_{cond,x,out}+q_{conv}+q_{rad} \tag{7}$$

The above equation, after substituting for the individual terms and simplification, leads to:

$$k_s t\frac{\partial^2 T}{\partial x^2}+k_f\left(\frac{\partial T}{\partial y}\right)_{y=0}+q_v t-\frac{\varepsilon}{1-\varepsilon}\left[\sigma T_i^4-J_i\right]=0 \tag{8}$$

Equation (8), after appropriate non-dimensionalisation, results in:

$$\frac{\partial^2\theta}{\partial X^2}+\gamma\left(\frac{\partial\theta}{\partial Y}\right)_{Y=0}+A_{r1}A_{r2}-\frac{\varepsilon}{1-\varepsilon}\gamma N_{RF}\left[\left(\frac{T_i}{T_\infty}\right)^4-J_i'\right]=0 \tag{9}$$

Here, γ and N_{RF} are the thermal conductance parameter and radiation-flow interaction parameter, respectively,

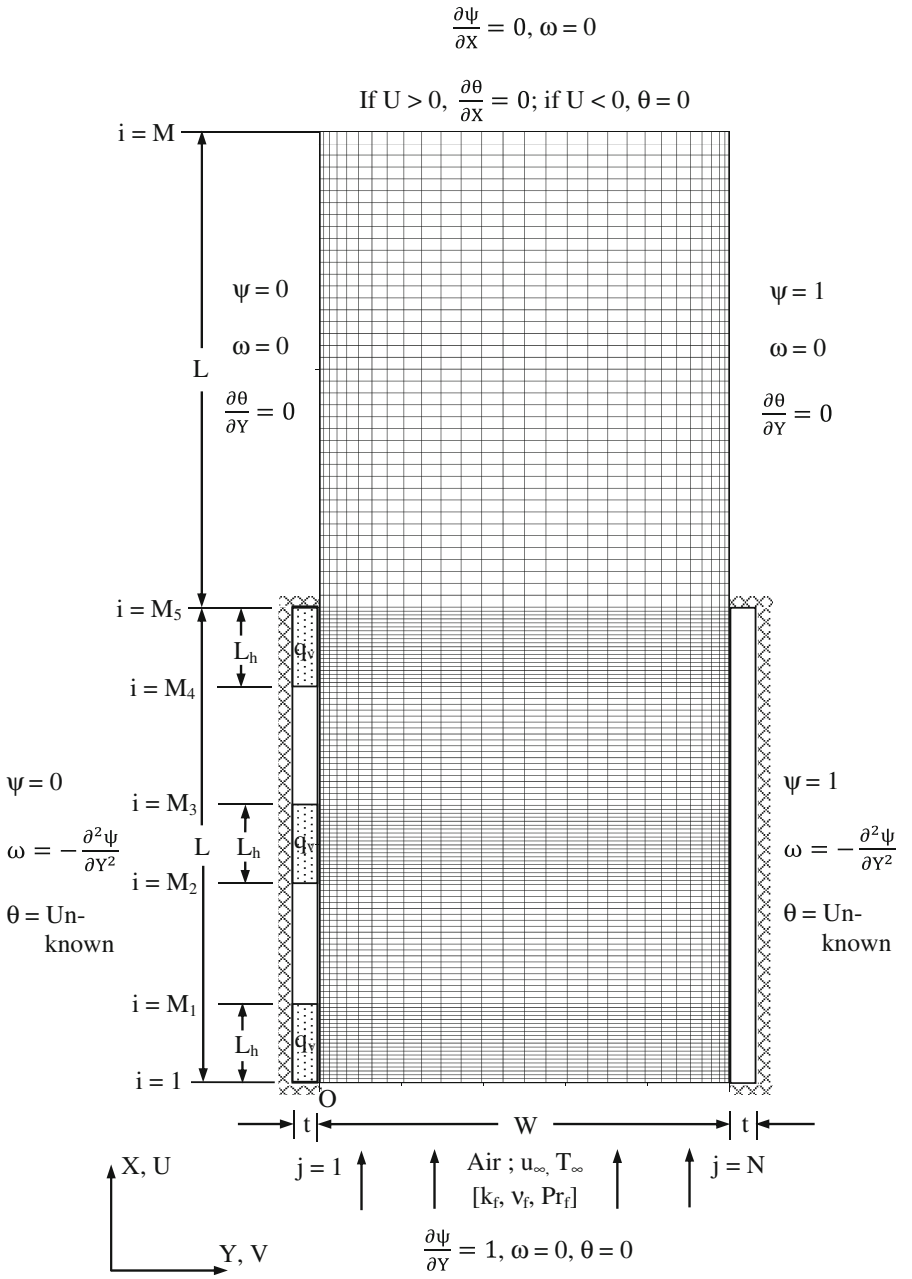

Fig. 2 Discretized computational domain along with pertinent boundary conditions used

while A_{r1} and A_{r2} are the two non-dimensional geometric parameters, as defined in nomenclature. J_i' is the non-dimensional radiosity of the ith element defined as $J_i/(\sigma T_\infty^4)$, where J_i is the radiosity that is defined as follows:

$$J_i = \varepsilon\sigma T_i^4 + (1-\varepsilon)\sum_{k=1}^{n} F_{ik}J_k \tag{10}$$

where n is the total number of elements of the enclosure pertaining to the four boundaries of the computational domain. The view factors needed in the above calculation are computed using the crossed string method of Hottel, the details of which are available in many references (e.g., Siegel and Howell [27]).

The energy balance related to the element at the interface between heat-source and non-heat source portions of the left wall looks similar to Eq. (7), with the only change coming in the heat generation term as only one half of the element pertains to heat source. With regard to the non-heat source portions of the left wall, the treatment would be similar as above with just the source term not present. Since the right wall does not possess any heat source, the same governing equation as applicable for the non-heat source portions of the left wall is valid with appropriate sign convention being followed. The governing equations for the top and bottom adiabatic ends of the walls of the channel are to be deduced separately. For example, the

energy balance on the element pertaining to the bottom adiabatic end of the left wall is:

$$q_{gen} = q_{cond,x,out} + q_{conv} + q_{rad} \tag{11}$$

Appropriate substitution of different terms in the above equation and simplification results in the following governing equation for the bottom adiabatic end of the left wall.

$$\frac{2}{\Delta x_{hs}} k_s t \frac{\partial T}{\partial x} + k_f \left(\frac{\partial T}{\partial y}\right)_{y=0} + q_v t - \frac{\varepsilon}{1-\varepsilon}\left[\sigma T_i^4 - J_i\right] = 0 \tag{12}$$

Non-dimensionalisation of the above equation in a manner similar to that discussed already gives rise to:

$$\frac{2}{\Delta X_{hs}} \frac{\partial \theta}{\partial X} + \gamma \left(\frac{\partial \theta}{\partial Y}\right)_{Y=0} + A_{r1} A_{r2} - \frac{\varepsilon}{1-\varepsilon} \gamma N_{RF} \left[\left(\frac{T_i}{T_\infty}\right)^4 - J_i'\right] = 0 \tag{13}$$

The rest of the boundary conditions pertaining to ψ, ω and θ are shown in Fig. 2.

3 Solution methodology and ranges of parameters

The governing non-dimensional Eqs. (4–6) are transformed into algebraic equations making use of the finite volume method that has been rigorously discussed in various references like Gosman et al. [28]. The advection terms pertaining to the above governing equations are tackled making use of second upwinding, the details of which could be had from the references like Roache [29]. The resulting algebraic equations are solved by the Gauss–Seidel iterative technique. With regard to relaxation used during iterations, it has been noticed that vorticity (ω) and stream function (ψ) need under relaxation with a relaxation parameter 0.3, while for temperature (θ), it would suffice to use full relaxation with relaxation parameter unity. The iterations are terminated when the convergence criteria, respectively, equal to 1×10^{-4}, 5×10^{-4} and 1×10^{-4} on ψ, ω and θ are met with.

Proper care has been taken in discretizing the computational domain as shown in Fig. 2. Cosine function has been chosen across the channel (Y direction) owing to the fact that the velocity and temperature gradients are quite steep at the vicinity of the two walls of the channel. In the axial (X) direction, though uniform grids are used all along, appropriate degree of fineness has been ensured for heat source portions and non-heat source portions of the channel wall and the extended domain. The above-mentioned unequispaced grid system for convection calculations has also been employed for evaluating the view factors and radiosities pertaining to radiation calculations in order to ensure the grid compatibility. All the open boundaries of the computational domain are considered to be black ($\varepsilon = 1$). A computer code in C^{++} is exclusively written to solve the present problem. The local velocities and the local temperatures pertaining to entire computational domain, which includes the temperatures along the two channel walls, are obtained upon solving the problem. The peak non-dimensional temperature (θ_{max}) is extracted from the local values of wall temperature, while the average non-dimensional temperature (θ_{av}) is calculated as: $\theta_{av} = \frac{1}{AR}\int_0^{AR} \theta(X)dX$. The relative contributions of mixed convection and radiation are obtained upon integrating the corresponding local values along the channel making use of the Simpson's 1/3 rule for non-uniform step sizes.

As mentioned already, all the calculations in the present study are performed making use of air ($Pr_f = 0.71$) as the cooling agent assuming it to be a radiatively transparent and Boussinesq medium. The height of the channel (L) is chosen to be 20 cm, while the thickness (t) of each channel wall is taken to be 1.5 mm. The height (L_h) of each of the three heat sources is taken equal to L/8 (2.5 cm). For the above height L of the channel fixed, the width or the spacing (W) of the channel is a variable depending on the AR, which is an important independent parameter in the present problem. The range of AR is taken to be from 4 to 20 based on certain experimental studies reported on cooling of electronic equipment and devices by Peterson and Ortega [30]. The surface emissivity (ε) of the channel is chosen to vary between 0.05 and 0.85 in view of the fact that the surfaces like polished aluminum have $\varepsilon = 0.05$ and behave as poor emitters (or good reflectors), while those with $\varepsilon = 0.85$, with black paint as a typical example, behave as good emitters (or poor reflectors). With regard to thermal conductivity (k_s) of the material of the channel, $0.25 \le k_s \le 1$ is chosen as appropriate since the printed circuit boards are typically composed of materials of thermal conductivity of the order of unity. An appropriate example for this is Mylar coated epoxy glass that has thermal conductivity equal to 0.26 W/m K. The modified Richardson number (Ri_w^*) is varied between 0.1 and 25, with the lower limit ($Ri_w^* = 0.1$) signifying the asymptotic forced convection limit, while the upper limit ($Ri_w^* = 25$) implies the asymptotic free convection limit. The above values of Ri_w^* are considered based on certain initial trials made with a class of values for the same. It has been noticed that a value of $Ri_w^* > 25$ lets the peak wall temperature to go beyond 150 °C, while a value less than 0.1 for Ri_w^* renders the peak wall temperature to go down below 30 °C. Since most of the electronic cooling applications have the peak device temperature varying between 30 and 120 °C, the above range for Ri_w^* appears to be quite justified.

4 Results and discussion

4.1 Grid sensitivity analysis

Before taking up the various parametric studies concerned with the present problem, it is customary to freeze on the best possible grid system to discretize the computational domain. An exhaustive grid sensitivity analysis has been carried out to serve the above purpose. The present section gives a summary of this analysis for a fixed input comprising $q_v = 5 \times 10^5$ W/m^3, $k_s = 0.25$ W/m K, AR = 12, $\varepsilon = 0.45$ and $Ri_w^* = 1$. The study is performed in four stages and the results are as given in Tables 1, 2, 3 and 4. In the first stage of the grid independence test (Table 1), the number of grids (M_5) along the left wall of the channel is varied holding the number of grids along the extended length of X direction (M–M_5) equal to 80 and the number of grids in the transverse (Y) direction equal to 61. As can be noticed, θ_{max} changes by 0.0685 % as M_5 increases from 121 to 151, while its change comes down to 0.0495 % with a further increase of M_5 to 181. However, a subsequent rise in M_5 to 211 makes the percentage change in θ_{max} to increase to 0.0591 %. In view of the above, the number of grids along the left as well as the right wall of the channel is frozen to be 181. In the second stage (Table 2), an attempt is made to fix the ratio of grid size in the heat source portion to that in the non-heat source portion of the left wall, holding M_5 at 181 (as already frozen) and with (M–M_5) and N remaining at 80 and 61, respectively. It can be noticed that the percentage change in θ_{max} continuously diminishes as the heat source to non-heat source grid ratio increases. However, a check for energy balance made reveals that the heat source to non-heat source grid ratio of 0.4444 fetches the best possible energy balance with the discrepancy between the heat generated and the heat dissipated restricted to 0.7181 %. Thus, the same is identified to be the best heat source to non-heat source grid ratio. Table 3 shows the results of the third stage where the total number of grids along the X direction (M) is varied holding M_5 and heat source to non-heat source grid ratio as 181 and 0.4444 (as frozen thus far) and further arbitrarily considering N to be equal to 61. The table reveals that M = 261 is the best option. In the fourth stage of grid independence test (Table 4), the number of grids across the channel (N) is varied with all other grid numbers held fixed as per the previous three stages. The table makes it obvious that the percentage change in θ_{max} progressively comes down as N is increased from 31 to 71, with change between N = 61 and N = 71 noticed to be quite meagre. Thus, N = 61 would be the best choice. In summary, the optimum grid structure would have M × N = 261 × 61, $M_1 = 25$, $M_2 = 79$, $M_3 = 103$, $M_4 = 157$ and $M_5 = 181$.

Table 1 First stage of grid independence test—to fix grids along the wall (M_5)

S. no.	M_5	M × N	θ_{max}	Percentage change (abs.)
1	91	171 × 61	0.842261	–
2	121	201 × 61	0.843638	0.1635
3	151	231 × 61	0.844216	0.0685
4	181	261 × 61	0.844634	0.0495
5	211	291 × 61	0.845133	0.0591

[$q_v = 5 \times 10^5$ W/m^3, $k_s = 0.25$ W/m K, $\varepsilon = 0.45$, AR = 12, $Ri_w^* = 1$] (M–M_5) = 80, N = 61

Table 2 Second stage of grid independence test—to fix the ratio of heat-source portion divisions (HS) to non-heat-source portion divisions (NHS)

S. no.	HS	NHS	Ratio, HS:NHS	θ_{max}	Percentage change in θ_{max} (abs.)	Percentage discrepancy in energy balance (abs.)
1	12	72	0.1666	0.870756	–	8.0171
2	16	66	0.2424	0.861607	1.051	4.8877
3	20	60	0.3333	0.852833	1.018	1.9894
4	24	54	0.4444	0.844634	0.961	0.7181
5	28	48	0.5833	0.837269	0.872	3.2605

[$q_v = 5 \times 10^5$ W/m^3, $k_s = 0.25$ W/m K, $\varepsilon = 0.45$, AR = 12, $Ri_w^* = 1$] $M_5 = 181$, M = 261, N = 61

Table 3 Third stage of grid independence test—to fix total grids along X direction (M)

S. no.	M × N	M_5	θ_{max}	Percentage change (abs.)
1	201 × 61	181	0.850458	–
2	221 × 61	181	0.846548	0.4598
3	241 × 61	181	0.845719	0.0979
4	261 × 61	181	0.844634	0.1283
5	281 × 61	181	0.844306	0.0388

[$q_v = 5 \times 10^5$ W/m^3, $k_s = 0.25$ W/m K, $\varepsilon = 0.45$, AR = 12, $Ri_w^* = 1$] $M_5 = 181$, N = 61

4.2 Check for mass and energy balance

The results of the present problem are checked for mass and energy balance in the entire mixed convection regime. For example, for a typical input comprising $q_v = 5 \times 10^5$ W/m^3, $k_s = 0.25$ W/m K, $\varepsilon = 0.45$ and AR = 12, results have been obtained for five values of Ri_w^* (viz., 0.1, 0.25, 1, 10 and 25). It is noticed that both the mass and the energy balance are satisfactory within ±0.15 and ±0.75 %, respectively. Trends similar to the above are noticed with regard to the rest of the input too.

Table 4 Fourth stage of grid independence test—to fix grids across the channel (N)

S. no.	M × N	M_5	θ_{max}	Percentage change (abs.)
1	261 × 31	181	0.839187	–
2	261 × 41	181	0.842285	0.3692
3	261 × 51	181	0.843921	0.1942
4	261 × 61	181	0.844634	0.0845
5	261 × 71	181	0.845083	0.0532

[$q_v = 5 \times 10^5$ W/m^3, $k_s = 0.25$ W/m K, $\varepsilon = 0.45$, AR = 12, $Ri_w^* = 1$] $M_5 = 181$, M = 261

4.3 Validation for velocity and temperature calculations

Aung and Worku [31, 32] have given equations for non-dimensional vertical velocity (U) and non-dimensional temperature (θ) for mixed convection in a vertical channel with symmetric and asymmetric wall temperatures. They assumed fully-developed flow and used boundary layer approximations while solving the governing fluid flow and energy equations. The present work, however, does not make these simplifying assumptions. Notwithstanding the above, an attempt has been made to compare the velocity and temperature profiles of the present study with those of Aung and Worku. They assumed the right wall to be hot and the left wall to be cold contrary to the present work where the left wall is hotter and the right wall is colder. Further, they have used Gr_w/Re_w as the governing mixed convection parameter in the place of Gr_w^*/Re_w^2. In view of the above, solution to the present problem too has been obtained by appropriately modifying the computer code written. It has been noticed that the exit velocity and temperature profiles of the present work pertaining to $Gr_w/Re_w = 0$, 100 and 250 exactly merge with those of Aung and Worku, while disparities are noticed towards larger values of Gr_w/Re_w. The assumption of a fully developed flow by Aung and Worku and the use of boundary layer approximations by them coupled with the possible onset of turbulence towards larger values of Gr_w/Re_w could be attributed to the above mismatch.

4.4 Validation for fluid flow results

Figure 3 shows (a) the non-dimensional vertical velocity and (b) the non-dimensional temperature profiles at the exit of the channel. The plots are drawn for a representative case, where there is a heat source in each wall with $q_V = 5 \times 10^5$ W/m^3, while k_s and ε are taken to be 0.5 W/m K and 0.45, respectively. Four different ARs (4, 8, 16 and 20), covering the range ($4 \le AR \le 20$), have been taken and the study is performed in the asymptotic forced convection limit ($Ri_w^* = 0.1$). It is seen from the figure that

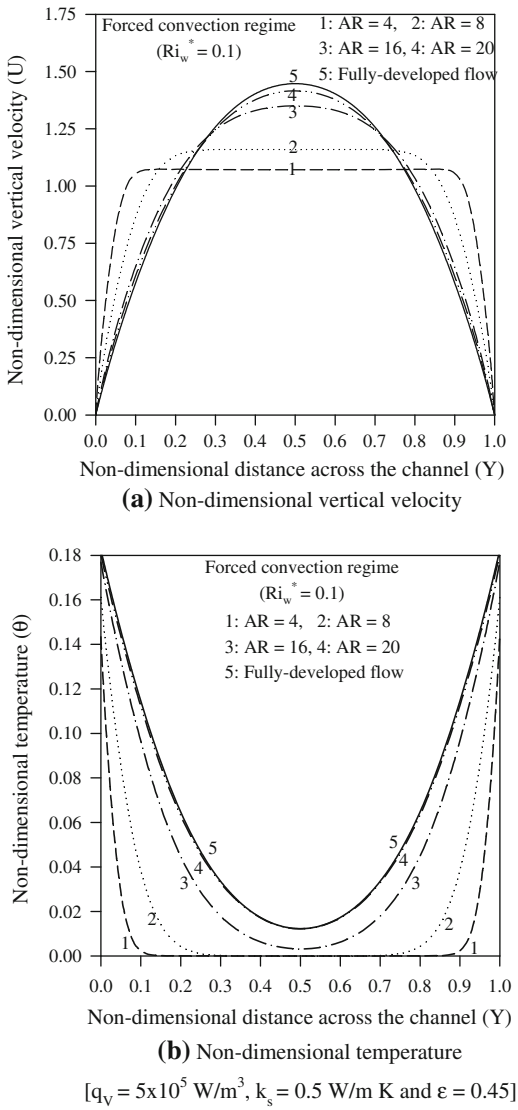

Fig. 3 Non-dimensional vertical velocity and temperature profiles at channel exit for different aspect ratios in the forced convection dominant regime

the flow is far from fully-developed for the lower values of AR. The velocity and temperature profiles do not merge with the fully-developed velocity and temperature profiles of plane-Poiseuille flow even for the highest aspect ratio (AR = 20) chosen in the present analysis. In view of these observations, the lowest aspect ratio (AR = 4) of the present analysis can be treated as the flat plate limit—implying that the two channel walls could be assumed isolated from each other.

Thus, the validation of the fluid flow results was made by comparing the mean friction coefficient calculations of the present work with the exact flat plate solution of Blasius [33] in the asymptotic forced convection limit ($Ri_w^* = 0.1$). To do this, a set of 15 data has been generated for $Ri_w^* = 0.1$ and for AR = 4. The $\bar{C}_f$ obtained from the

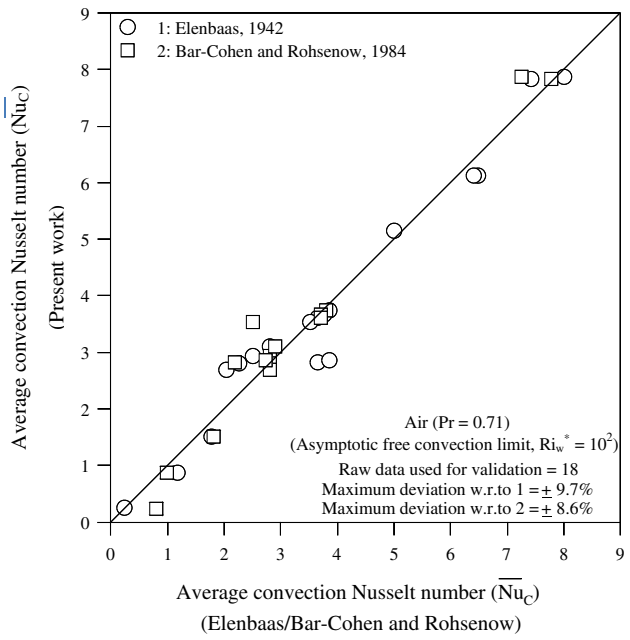

Fig. 4 Validation for average convection Nusselt number with the available results in the asymptotic free convection limit

present work compared well with the Blasius value of $\bar{C}_f$ with a maximum deviation of ±7.8 %. Subsequently, a correlation has been evolved for, $\bar{C}_f$ based on the above 15 data, as: $\bar{C}_f = 5.5714\ Re_L^{-0.6392}$, which has a correlation coefficient of 0.999 and an error band of ±0.89 %. This correlation has subsequently been modified, by adjusting the exponent of Re_L to −0.5, as: $\bar{C}_f = 1.382\ Re_L^{-0.5}$. This implies a difference of ±4.1 % between the present correlation and the exact solution of Blasius [33]. Keeping in mind that $Ri_w^* = 0.1$ is only an asymptotic forced convection limit for the present problem with a varying wall temperature, while the Blasius solution is for forced convection from an isothermal flat plate, this is indeed a very good match. This validates the fluid flow related calculations of the present study.

4.5 Validation for heat transfer results

In order to validate the heat transfer results, the complexity in the present problem has been degenerated to the special case, wherein the two walls of the channel do not contain any heat sources and are isothermal. A numerical experiment has been conducted with a set of 18 data generated encompassing the entire range of aspect ratios (AR = 4 to 20) for $Ri_w^* = 100$, which, incidentally, is far larger than the asymptotic free convection limit for the present study (viz., $Ri_w^* = 25$). The average convection Nusselt number thus evolved is compared with semi-empirical correlation of Elenbaas [1] and the analytical solution of Bar-Cohen and Rohsenow [4], both of which are for free convection in air in a vertical channel with symmetric isothermal walls, as shown in Fig. 4. A fairly good agreement has been noticed with maximum deviations restricted to within ±9.7 and ±8.6 %, respectively.

4.6 Variation of local temperature distribution with surface emissivity

Figure 5a, b depict the nature of variation of the local non-dimensional temperature, θ(X), along the left and the right walls of the channel, respectively, for three different surface emissivities (ε = 0.05, 0.45 and 0.85). The study is made for a fixed set of the rest of the input parameters, viz., $q_v = 5 \times 10^5$ W/m^3, $k_s = 0.25$ W/m K, AR = 12 and $Ri_w^* = 25$. It is to be noted that only the left wall of the channel contains flush-mounted discrete heat sources along its length, while the right wall merely acts as a heat sink. Figure 5a shows that, for a given ε, the local left wall temperature increases very sharply as one moves from the entry of the channel. It reaches a local maximum somewhere near the end of the first heat source. It subsequently decreases, which continues along the non-heat source portion between the first and the second heat sources. After reaching a local minimum just ahead of the second heat source, the temperature shoots up again and reaches a second local peak towards the fag end of the second heat source. The temperature comes down once again as one moves through the second non-heat source portion between the second and third heat sources. After reaching second local minimum, θ(X) sharply increases once again, reaching its third peak near the top adiabatic end of the wall. The above nature of variation, understandably, is on account of discreteness in heat generation in the wall with heat source and non-heat source portions present alternately. It can also be noticed that the three local peaks in θ(X) are in the ascending order with the overall maximum (θ_{max}) occurring at the top adiabatic end of the wall. The figure further shows the effect of surface emissivity of the channel (ε) in controlling the local wall temperature, with the local temperature decreasing for an increasing ε. This, obviously, is owing to enhanced radiative dissipation from the wall. In the present study, for example, the second local peak along the wall decreases by 17.73 % as ε is increased to 0.85 from 0.05.

Figure 5b demonstrates the effect of ε on right wall temperature distribution. For any given ε, one can notice a waviness in the local right wall temperature, which is a direct consequence of the waviness discussed with regard to the left wall temperature. Further, here, an increase in ε, increases the local right wall temperature. This may be attributed to the enhanced rate of irradiation received by the right wall from the left wall. In the present study, the local temperature at the top adiabatic end of the right wall is shooting up by 41.78 % as a consequence of a rise in ε from 0.05 to 0.85.

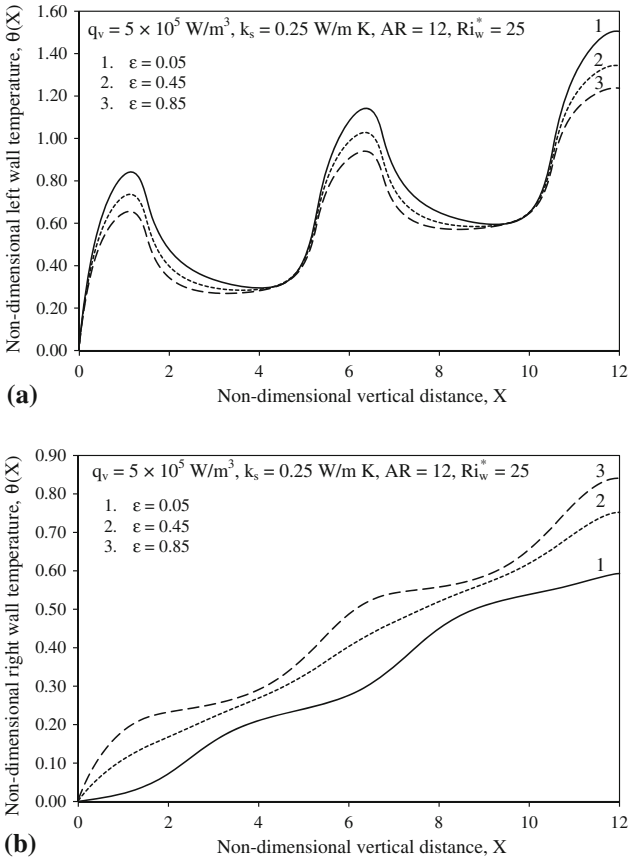

Fig. 5 Local non-dimensional temperature profiles for **a** left wall and **b** right wall for different surface emissivities

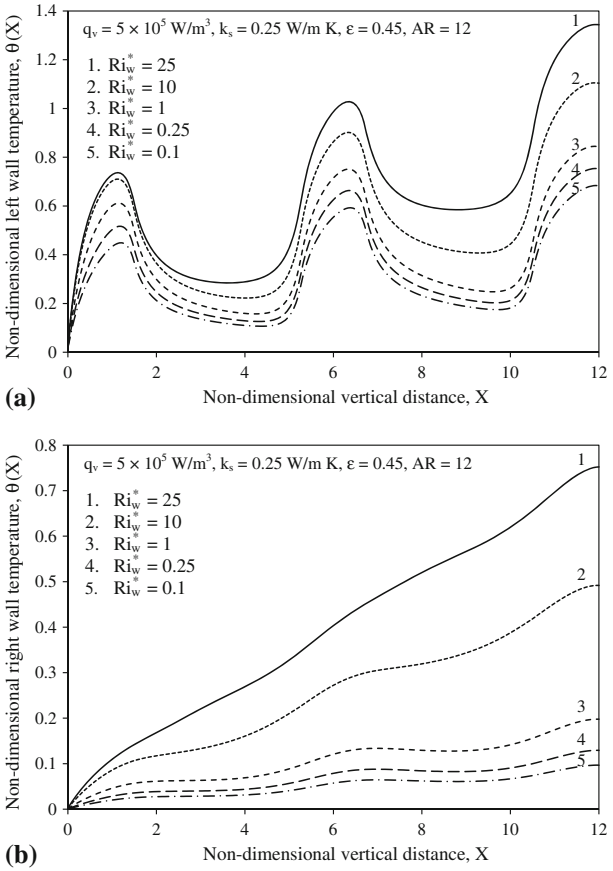

Fig. 6 Local non-dimensional temperature profiles for **a** left wall and **b** right wall in various regimes of mixed convection

4.7 Variation of local temperature distribution in different regimes of mixed convection

In order to examine the nature of local temperature profiles of the two walls of the channel in different regimes of mixed convection, a study is performed for a fixed input of $q_v = 5 \times 10^5$ W/m^3, $k_s = 0.25$ W/m K, $\varepsilon = 0.45$ and AR = 12. Five different values of modified Richardson number (Ri_w^*) are chosen encompassing the whole mixed convection regime and they include $Ri_w^* = 0.1$, which signifies an asymptotic limit of forced convection, $Ri_w^* = 1$, which indicates pure mixed convection and $Ri_w^* = 25$ that pertains to an asymptotic limit of free convection. Figure 6a, b, respectively, indicate the families of temperature profiles pertaining to left and right walls of the channel. It could be clearly seen that the general nature of variation of local temperature either along the left or along the right wall of the channel is similar to what has been noticed in Fig. 5a, b. In particular, Fig. 6a indicates that the local temperature along the left wall decreases, rather sharply, to begin with and mildly subsequently, as the flow regime transits from free convection to forced convection via pure mixed convection, with the drop in local temperature being larger between $Ri_w^* = 25$ and $Ri_w^* = 1$ when compared to that between $Ri_w^* = 1$ and $Ri_w^* = 0.1$. In the present example, θ at the channel exit along the left wall is coming down by 37.21 % as Ri_w^* decreases from 25 to 1. As against this, for a subsequent drop in Ri_w^* to 0.1 from 1, θ at the same location comes down only by 19.01 %.

With regard to the right wall of the channel, as noticeable from Fig. 6b, there is a large drop in local temperature as Ri_w^* decreases from 25 to 1. The temperature though decreases with a further decrease in Ri_w^* from 1 to 0.1, the degree of decrease is not as eminent as it has been earlier. In the present example, the right wall temperature at the channel exit decreases by 73.69 % as Ri_w^* decreases from 25 to 1, while it gets decreased only by 51.12 % as Ri_w^* further decreases to 0.1 from 1.

4.8 Exclusive effect of surface radiation on local temperature distribution

In order to separate out the exclusive role surface radiation plays in influencing the local temperature distribution along the left wall of the channel, a study is conducted for

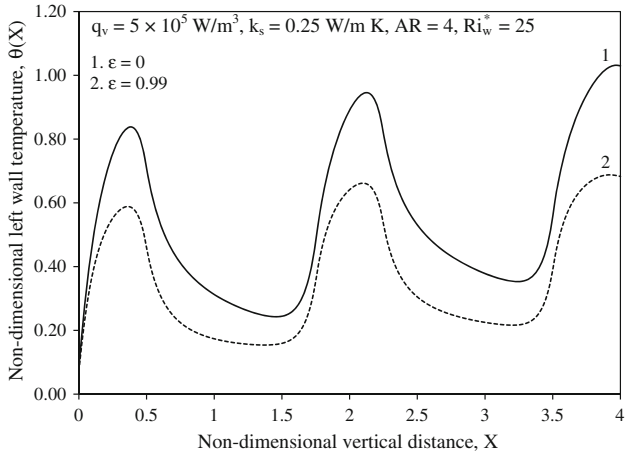

Fig. 7 Demonstration of exclusive effect of radiation on non-dimensional local left wall temperature of the channel

$q_v = 5 \times 10^5$ W/m^3, $k_s = 0.25$ W/m K, AR = 4 and $Ri_w^* = 25$. Two limiting values of ε, viz., 0 and 0.99 are chosen to represent cases (1) without radiation and (2) with maximum possible radiation. The appropriate surfaces for the above two cases could be taken to be, respectively, very highly polished factory fresh aluminum sheet and lamp black soot. Figure 7 shows the result obtained. One can clearly notice a considerable drop in the local temperature along the left wall when once the highly reflecting and poorly emitting surface (ε = 0) is replaced by the best possible emitter (ε = 0.99). This effect is more pronounced in the heat source portions of the wall where major heat transfer activity is there. In the present study, the temperature at the top adiabatic end of the left wall, for example, drops down by 21.05 % by the above exercise. This clearly underlines the need for taking radiation into reckoning in the present problem.

4.9 Local wall temperature profiles with different heat source configurations

The present problem geometry consists of three identical heat sources in the left wall of the channel. It would be interesting to see the nature of variation of local temperature distribution along the left wall for this configuration in comparison to configurations that have any one of the three heat sources present. Keeping the above in mind, results are obtained for fixed input of $q_v = 5 \times 10^5$ W/m^3, $k_s = 0.25$ W/m K, ε = 0.85, AR = 12 and $Ri_w^* = 25$. The four configurations chosen are, respectively, (1) all heat sources present, (2) bottommost heater alone present, (3) central heater alone present and (4) topmost heat source alone present. Figure 8 shows the results of this study. As understandable, configuration 1 is the one discussed already in the previous results and thus the temperature

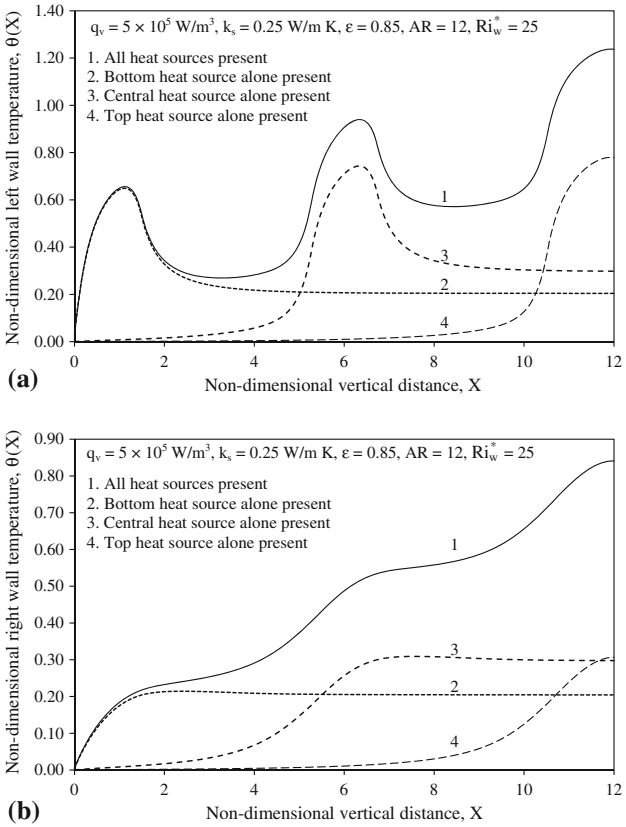

Fig. 8 Local temperature profiles for **a** left wall and **b** right wall with different heat source configurations used

profile (curve 1) resembles what has been noticed already in those results. In configuration 2 (curve 2), with only the bottommost heat source present, the temperature increases sharply reaching its maximum just ahead of the top end of the heat source. It drops down again rather sharply to begin with before getting asymptotic thereafter. This is because of the absence of the remaining two heat sources in the present configuration which makes the rest of the left wall after the first heat source to behave like a fin (heat sink). In the third configuration with central heat source alone present, the temperature rises very mildly till the heat source is reached, before shooting up sharply reaching its maximum again just ahead of the top end of the heat source. The temperature, like in configuration 2, now decreases sharply initially and after crossing the heat source it gets asymptotic in the remaining portion of the wall owing to reasons already explained. Since configuration 4 has only the topmost heat source present, the temperature rise is very meager almost up to the start of the heat source. It shoots up in the heat source reaching its peak just ahead of the top end of the heat source, which incidentally is the top adiabatic end of the channel wall. It can be seen from the figure that, if one were to use a single heat source in the channel, the best position would be the

bottommost end of the wall, while the least preferred position is the top end of the wall keeping in mind that the objective here is the control of peak temperature attained by the channel.

4.10 Variation of maximum channel temperature with surface emissivity in different regimes of mixed convection

Figure 9 shows the interactive effect of surface radiation on mixed convection in influencing the maximum non-dimensional temperature (θ_{max}) of the channel. The study is made for a fixed input of $q_v = 5 \times 10^5$ W/m^3, $k_s = 0.25$ W/m K, AR = 20. Five different values of ε and Ri_w^* are chosen as shown. For a given ε, θ_{max} decreases with decrease in Ri_w^* as a consequence of the transit of the flow regime from free to forced convection. However, the above effect is found to be quite eminent in the free convection dominant regime ($1 < Ri_w^* \leq 25$), while it peters down in the forced convection dominant regime ($0.1 \leq Ri_w^* < 1$). In the present example, for $\varepsilon = 0.45$, θ_{max} comes down by a huge 54.89 % as Ri_w^* decreases from 25 to 1. In contrast, it comes down by only 27.96 % as Ri_w^* further decreases to 0.1 from 1. The figure also shows that θ_{max} decreases almost monotonically with increase in ε for a given Ri_w^*. The above effect of ε on θ_{max} is noticed to be at its best in the asymptotic forced convection limit ($Ri_w^* = 0.1$), while it diminishes towards the asymptotic free convection limit ($Ri_w^* = 25$). This is further substantiated by the observation made with regard to radiative heat dissipation, which is found to be increasing largely for $Ri_w^* = 0.1$ than for $Ri_w^* = 25$ with ε increasing from 0.05 to 0.85 in both the cases. In the present example, θ_{max} is decreasing, respectively, by 23.15, 20.66 and 13.49 % for $Ri_w^* = 0.1$, 1 and 25 as ε increases from 0.05 to 0.85.

4.11 Exclusive effect of radiation on peak channel temperature

The explicit contribution exhibited by radiation in influencing the peak temperature assumed by the channel is shown in Fig. 10 for a given set of data (q_v, k_s and AR). The bulk errors that creep in while calculating θ_{max} are quite evident in different regimes of mixed convection considered. Any attempt that ignores radiation and considers only mixed convection overestimates θ_{max} quite unacceptably. In the asymptotic free convection limit ($Ri_w^* = 25$), θ_{max} comes down by 33.31 % by just changing the channel surface from perfect reflector ($\varepsilon = 0$) to perfect emitter ($\varepsilon = 0.99$). Even in the asymptotic forced convection limit ($Ri_w^* = 0.1$), the effect of ε is quite significant with θ_{max} decreasing by as much as 29.54 % due to the above exercise.

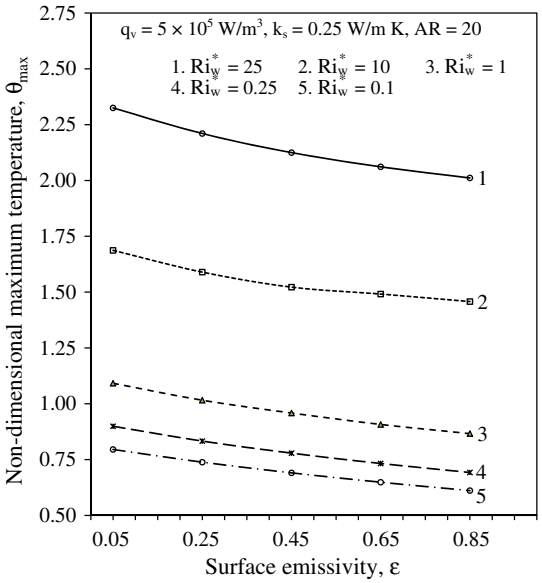

Fig. 9 Variation of non-dimensional maximum temperature of the channel with surface emissivity in various regimes of mixed convection

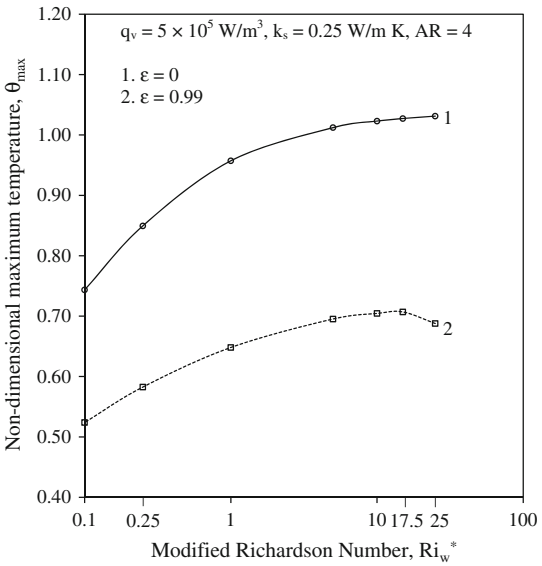

Fig. 10 Exclusive effect of radiation on peak channel temperature in different regimes of mixed convection

4.12 Effect of aspect ratio on maximum channel temperature

One of the important independent parameters concerning the present problem configuration is the AR of the channel. It is already mentioned that, with the height (L) of the channel fixed, a changing AR alters the channel width (W), with decrease in AR implying a wider channel and an increase in AR corresponding to a narrower channel. Figure 11 brings out the role AR plays in influencing θ_{max} for

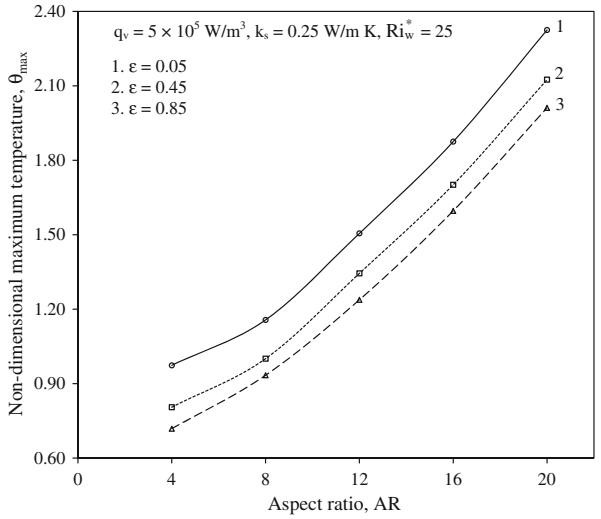

Fig. 11 Variation of maximum temperature of the channel with aspect ratio for different surface emissivities

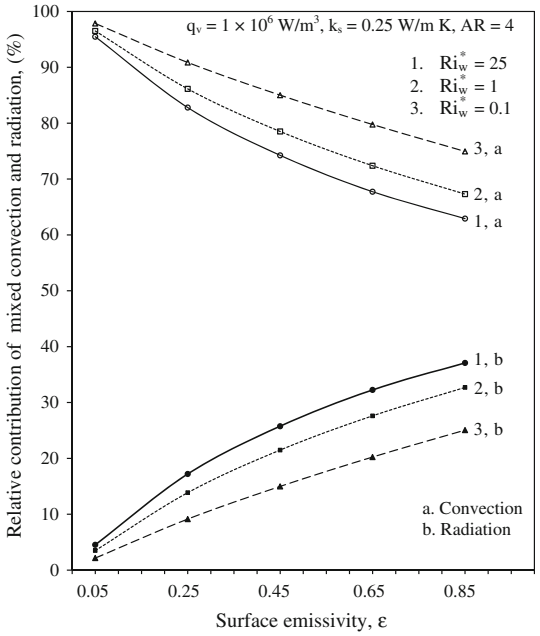

Fig. 12 Relative contributions of mixed convection and radiation in channel heat dissipation with surface emissivity in typical regimes of mixed convection

three typical surface emissivities of the channel and for a given fixed set of the remaining input. For a given ε, θ_{max} is increasing quite sharply with increasing AR. The above effect is getting more pronounced as one selects channel of larger surface emissivity. In the present case, for $\varepsilon = 0.05$, a change in AR from 4 to 20 shoots up θ_{max} by 138.74 %, while, for $\varepsilon = 0.85$, the above exercise is showing an increased effect on θ_{max} with its value rising by 179.93 %. The figure also shows a decrease in θ_{max}, for a given AR, with increase in ε. Again here, the drop in θ_{max} is larger between $\varepsilon = 0.05$ and $\varepsilon = 0.45$ than that between $\varepsilon = 0.45$ and $\varepsilon = 0.85$. Here, for AR = 12, θ_{max} is decreasing by 10.72 and 7.92 %, respectively, between the two limiting ranges of ε mentioned above. This study hints that it is unwise to pack the walls of a channel too closely as it results in an undue increase in the cooling load to be carried by the thermal control system concerned.

4.13 Variation of relative contributions of mixed convection and radiation with surface emissivity in different regimes of mixed convection

The heat generated in the discrete heat sources that are flush-mounted in the left wall gets conducted along the wall and subsequently gets dissipated by the combined modes of mixed convection and radiation. It would be useful to separate out the contributions from mixed convection and radiation to judge on the relative dominance of one over the other.

Figure 12 shows the percentage contributions from mixed convection and radiation plotted against surface emissivity (ε) of the channel in three typical regimes of mixed convection. The study is performed for a fixed input set of q_v, k_s and AR shown. The figure clearly shows that radiation, in general, takes part in heat dissipation in any given regime of convection. However, for a given ε, its role assumes significance as one moves towards the free convection dominant regime. Likewise, in a given regime, the role of radiation starts getting pronounced with increase in ε. In the present study, for example, even in the asymptotic forced convection limit ($Ri_w^* = 0.1$), just an increase in ε from 0.05 to 0.85 is increasing the contribution of radiation from 2.1 to 25.1 %, with a corresponding drop in the share from mixed convection. The same exercise in asymptotic free convection limit ($Ri_w^* = 25$) is increasing radiative dissipation from the channel from 4.5 to 37.1 %. This clearly underlines the need to take radiation into reckoning in all regimes of convection, in general, and while operating in free convection dominant regime, in particular.

4.14 Variation of relative contributions of mixed convection and radiation with aspect ratio in different regimes of mixed convection

The relative contributions of mixed convection and radiation in dissipating heat from the channel are plotted against AR of the channel for three typical values of Ri_w^* as shown in Fig. 13. The remaining input parameters, viz., q_v, k_s and ε, are maintained constant for the entire study as shown in the figure. The figure reveals a non-monotonic nature of variation of relative contributions due to both mixed convection and radiation with AR, in all the regimes of mixed convection, excepting for pure mixed convection ($Ri_w^* = 1$). In pure mixed convection regime, the

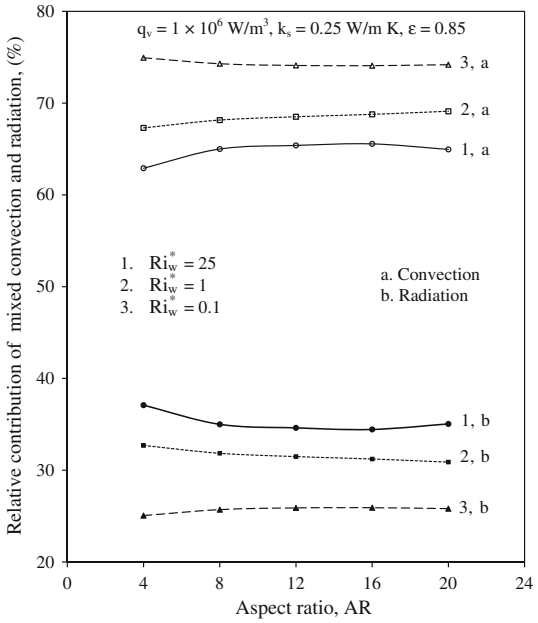

Fig. 13 Relative contribution of mixed convection and radiation with aspect ratio of the channel in various regimes of mixed convection

convective heat dissipation is increasing, though mildly, with AR, with a corresponding mirror-image decrease in the contribution from radiative dissipation. In the present example, the contribution from convection is increasing from 67.3 % for AR = 4 to 69.11 % for AR = 20, while that from radiation is dropping down to 30.89 % from 32.7 % between the same limits of AR. However, for $Ri_w^* = 25$ (asymptotic free convection limit), convective dissipation increases as AR increases from 4 to 16 before slightly dropping down as AR is further increased to 20. Obviously, the role played by radiation changes in accordance with that by convection. With regard to asymptotic forced convection limit ($Ri_w^* = 0.1$), convection contribution is diminishing, though very slightly, as AR is increased from 4 to 16, before rising very slightly due to a further rise in AR to 20. Again here, changes appropriate to the above are noticed vis-à-vis the role played by radiation.

4.15 Variation of relative contributions of mixed convection and radiation with thermal conductivity of channel material in different regimes of convection

The interplay between Ri_w^* and k_s in deciding the relative roles of mixed convection and radiation in heat dissipation from the channel is studied for a fixed input of q_v, ε and AR, as shown in Fig. 14. It is seen that, for $Ri_w^* = 1$ (pure mixed convection), an increasing k_s brings a very meager rise in the contribution from mixed convection with a corresponding decrease in that from radiation. However, as one moves towards either asymptotic free convection ($Ri_w^* = 25$) or asymptotic forced convection ($Ri_w^* = 0.1$) limit, a difference in the trend is noticed. Here, the convective dissipation decreases, comparatively by a larger degree than noticed above, as k_s increases from 0.25 to 1 W/m K. This is obviously followed by an appropriate rise in radiative dissipation. In the present example, for $Ri_w^* = 1$, convection dissipation is increasing from 69.11 to 69.72 %, while radiation contribution is coming down from 30.89 to 30.28 % as k_s increases between the above limits. In contrast, say for $Ri_w^* = 25$, convection is decreasing from 64.96 % for $k_s = 0.25$ W/m K to 62.46 % for $k_s = 1$ W/m K. Radiation, in turn, is increasing its contribution from 35.04 to 37.54 % during the above exercise. The figure further shows that there is an expected increase in radiative heat dissipation with the flow transiting from forced to free convection asymptotic limit with a corresponding mirror-image drop in the role of convection. In the present study, for $k_s = 0.625$ W/m K, radiation is increasing its effect in heat dissipation from 27.11 % for $Ri_w^* = 0.1$ to 36.32 % for $Ri_w^* = 25$.

5 Concluding remarks

The problem of conjugate mixed convection with radiation from a vertical channel with three identical flush-mounted discrete heat sources in the left wall has been numerically solved. A computer code is exclusively written for the purpose. A number of parametric studies elucidating the roles of surface emissivity, thermal conductivity of the walls of the channel, modified Richardson number and AR of the channel in influencing the various pertinent results of the problem have been performed. Certain conclusions have been drawn, some of which include:

1. The local left and right wall temperatures of the channel have been found to be, respectively, decreasing and increasing with increasing surface emissivity with other parameters held fixed. On the average, a change in the surface coating of the channel from poor to good emitter ($\varepsilon = 0.05$–0.85) has been found to be bringing down the peak channel temperature by 18–22 %. Further, the same exercise of change in ε as above is found to rise the right wall temperature by 40–42 %.
2. The results have been obtained by considering all the three heat sources and also by considering the bottommost, the central and the topmost heat source alone. It is noticed that, if one were to use a single heat

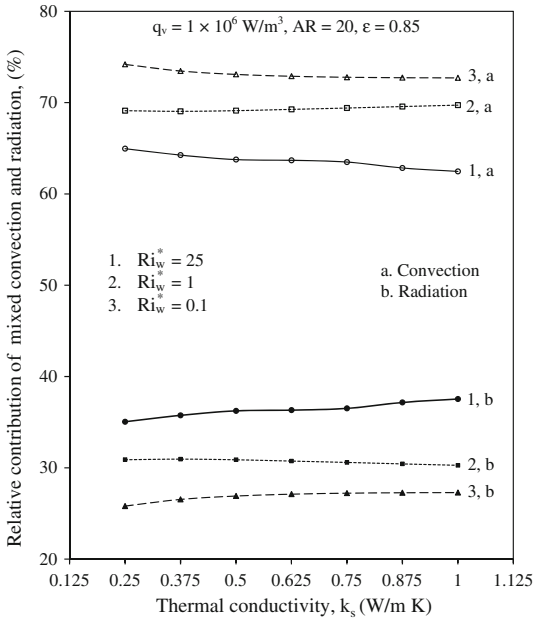

Fig. 14 Relative contributions of mixed convection and radiation with thermal conductivity of the channel material in different regimes of mixed convection

source in the channel, the most preferred position would be the bottommost end of the wall with the top end of the wall being the least preferred position, keeping in mind the control of peak temperature assumed by the channel.

3. The exclusive effect of surface radiation both on local and peak temperatures of the channel has been exhaustively studied. It is noticed that radiation plays a distinct role in thermal control of the channel in the entire mixed convection regime with the peak channel temperature coming down, respectively, by 34 and 30 % in the asymptotic free and forced convection limits when once radiation is taken into reckoning with $\varepsilon = 0.99$ (perfect emitter).
4. A study of the effect of AR on the results pointed out that it is unwise to pack the walls of the channel too closely as it unduly increases the cooling load on the thermal control system.
5. The relative contributions of mixed convection and radiation have been studied in great detail. A clear need to take radiation into reckoning in all regimes of convection, in general, and in free convection dominant regime, in particular, is noticed.
6. The variation of relative contributions of mixed convection and radiation with AR has been found to be non-monotonic in all the regimes of mixed convection barring the regime of pure mixed convection.

References

1. Elenbaas W (1942) Heat dissipation of parallel plates by free convection. Physica 9:1–28
2. Tao LN (1960) On combined free and forced convection in channels. ASME J Heat Transf 82:233–238
3. Quintiere J, Mueller WK (1973) An analysis of laminar free and forced convection between finite vertical parallel plates. ASME J Heat Transf 95:53–59
4. Bar-Cohen A, Rohsenow WM (1984) Thermally optimum spacing of vertical natural convection cooled parallel plates. ASME J Heat Transf 106:116–123
5. Aung W, Worku G (1987) Mixed convection in ducts with asymmetric wall heat fluxes. ASME J Heat Transf 109:947–951
6. Hamadah TT, Wirtz RA (1991) Analysis of laminar fully developed mixed convection in a vertical channel with opposing buoyancy. ASME J Heat Transf 113:507–510
7. Barletta A (1998) Laminar mixed convection with viscous dissipation in a vertical channel. Int J Heat Mass Transf 41:3501–3513
8. Carpenter JR, Briggs DG, Sernas V (1976) Combined radiation and developing laminar free convection between vertical flat plates with asymmetric heating. ASME J Heat Transf 98:95–100
9. Anand NK, Kim SH, Aung W (1990) Effect of wall conduction on free convection between asymmetrically heated vertical plates: uniform wall temperature. Int J Heat Mass Transf 33:1025–1028
10. Kim SH, Anand NK (1994) Laminar developing flow and heat transfer between a series of parallel plates with surface-mounted discrete heat sources. Int J Heat Mass Transf 37:2231–2244
11. Watson JC, Anand NK, Fletcher LS (1996) Mixed convective heat transfer between a series of vertical parallel plates with planar heat sources. ASME J Heat Transf 118:984–990
12. Gururaja Rao C, Balaji C, Venkateshan SP (2002) Effect of surface radiation on conjugate mixed convection in a vertical channel with a discrete heat source in each wall. Int J Heat Mass Transf 45:3331–3347
13. Gururaja Rao C, Balaji C, Venkateshan SP (2003) Conjugate mixed convection with surface radiation in a vertical channel with symmetric and uniform wall heat generation. Int J Transp Phenom 5:75–101
14. Olsson C-O (2004) Prediction of Nusselt number and flow rate of buoyancy driven flow between vertical parallel plates. ASME J Heat Transf 126:97–104
15. Campo A, Manca O, Morrone B (2006) Numerical investigation of the natural convection flows for low-Prandtl fluids in vertical parallel-plates channel. ASME J Appl Mech 73:96–107
16. Gururaja Rao C (2007) Interaction of surface radiation with conduction and convection from a vertical channel with multiple discrete heat sources in the left wall. Numer Heat Transf A 52:831–848
17. Guimaraes PM, Menon GJ (2008) Combined free and forced convection in an inclined channel with discrete heat sources. Int Comm Heat Mass Transf 35:1267–1274
18. Ermolaev IA, Zhbanov AI (2009) Mixed convection in a vertical channel with discrete heat sources at the wall. Fluid Dyn 44:511–516
19. Ramjee R, Satyamurty VV (2010) Local and average heat transfer in the thermally developing region of an asymmetrically heated channel. Int J Heat Mass Transf 53:1654–1665
20. Terekhov VI, Ekaid AL (2011) Laminar natural convection between vertical isothermal heated plates with different temperatures. J Eng Thermophys 20:416–433
21. Sakurai A, Matsubara K, Takakuwa K, Kanbayashi R (2012) Radiation effects on mixed turbulent natural and forced convection in a horizontal channel using direct numerical simulation. Int J Heat Mass Transf 55:2539–2548

22. Al-Amri FG, El-Shaarawi MAI (2012) Mixed convection with surface radiation between two asymmetrically heated vertical parallel plates. Int J Thermal Sci 58:70–78
23. Alves TA, Altemani CAC (2012) An invariant descriptor for heaters temperature prediction in conjugate cooling. Int J Thermal Sci 58:92–101
24. Amirouche Y, Bessaïh R (2012) Three-dimensional numerical simulation of air cooling of electronic components in a vertical channel. Fluid Dyn Mater Process 8:295–309
25. Madhusudhana G (2012) Natural convection in a vertical channel with arrays of flush-mounted heaters on opposite conductive walls. Numer Heat Transf A 62:111–135
26. Li R, Bousetta M, Chénier E, Lauriat G (2013) Effect of surface radiation on natural convective flows and onset of flow reversal in asymmetrically heated vertical channels. Int J Thermal Sci 65:9–27
27. Siegel R, Howell JR (1992) Thermal radiation heat transfer. Taylor and Francis, Washington
28. Gosman AD, Pun WM, Runchal AK, Spalding DB, Wolfshtein M (1969) Heat and mass transfer in recirculating flows, 1st edn. Academic Press, London, pp 89–137
29. Roache PJ (1972) Computational fluid dynamics, 1st edn. Hermosa, Albuquerque, pp 15–207
30. Peterson GP, Ortega A (1990) Thermal control of electronic equipment and devices. In: Hartnett JP, Irvine TF Jr (eds) Advances in heat transfer. Academic Press Inc., San Diego, pp 181–314
31. Aung W, Worku G (1986) Developing flow and flow reversal in a vertical channel with asymmetric wall temperatures. ASME J Heat Transf 108:299–304
32. Aung W, Worku G (1986) Theory of fully developed combined convection including flow reversal. ASME J Heat Transf 108:485–488
33. Blasius H (1908) Grenzschichten in Flussigkeiten mit kleiner Reibung. Z Math Phys 56:1